JOURNAL OF MATERIALS SCIENCE 15 (1980) 1265–1275

Texture dependent stress corrosion failure of commercial titanium sheets in bromine-methanol solution

H. V. SUDHAKER NAYAK
Karnataka Regional Engineering College, Surathkal, India

K. I. VASU, Y. V. R. K. PRASAD
Department of Metallurgy, Indian Institute of Science, Bangalore, India

The stress corrosion cracking (SCC) characteristics of α-titanium sheets in a bromine-methanol solution have been studied in the annealed and cold-rolled conditions using longitudinal and transverse specimens. The times to failure for annealed longitudinal specimens were longer than those for similarly tested transverse specimens. The cold-rolled specimens developed resistance to SCC, but failed by cleavage when notched, unlike the intergranular separation in annealed titanium. The apparent activation energy was found to be texture dependent and was in the range 30 to 51 kJ mol^{-1} for annealed titanium, and 15 kJ mol^{-1} for cold-rolled titanium. The dependence of SCC behaviour on the texture is related to the changes in the crack initiation times. These are caused by changes in the passivation and repassivation characteristics of the particular thickness plane. The thickness planes are identified with the help of X-ray pole figures obtained on annealed and cold-rolled material. On the basis of the activation energy and the electrochemical measurements, the mechanism of SCC in annealed titanium is identified to be the one involving stress-aided anodic dissolution. On the other hand, the results on the cold-rolled titanium are in support of the hydrogen embrittlement mechanism consisting of hydride precipitation. The cleavage planes identified from the texture data match with the reported habit planes for hydride formation.

1. Introduction

It is well known that α-titanium and its α-alloys are susceptible to stress corrosion cracking (SCC) in organic media like methanol–halogen, in aqueous media like sea water or acids, and in hot salts like chlorides and nitrates. In methanolic solution containing halogen, halides or free acidity, α-titanium shows a tendency to crack along an intercrystalline path. The influence of electrochemical, metallurgical and mechanical parameters on the SCC characteristics of titanium and its alloys has been extensively studied and reviewed [1]. While a mechanism involving hydrogen embrittlement has been advocated for the SCC in α–β alloys, the mechanism of SCC in unalloyed annealed titanium has not been established unequivocally. The following models, however, have been suggested:

(a) stress-assisted localized anodic dissolution at grain boundaries [2, 3],

(b) selective adsorption of the halide ion at the stressed region of the metal at the crack tip lowering the interatomic bonding strength sufficiently to cause rupture of bond and an increment of crack growth [4];

(c) hydrogen embrittlement owing to hydride precipitation on operative slip planes [5].

In recent years, the role of crystallographic texture in causing SCC in titanium and its alloys has received some attention [1, 6–10]. In α–β alloys it was reported [8, 9] that the threshold plane strain fracture toughness under SCC conditions (K_{ISCC}) is much lower than the fracture toughness (K_{IC}) when the texture is such that the basal planes are heavily stressed. Moreover, the longitudinal and transverse specimens had the

0022–2461/80/051265–11$03.10/0

K_{ISCC} values with about two-to-one difference. In α-titanium, however, the influence of texture on SCC has not been studied in detail. Previous investigations [11] have indicated that the cold-rolling texture in titanium sheets would render it immune to SCC and the material fails by cleavage when notched.

The aim of the present investigation is to study the influence of texture on the SCC characteristics and its possible effect on the mechanism of failure in α-titanium. Studies have been made on annealed as well as cold-rolled titanium sheets as the textures in these two conditions are known to be different. The approach has been to compare the behaviour of the longitudinal specimens with the transverse ones in both annealed and cold-rolled materials.

2. Experimental details

2.1. Material and specimen preparation

Commercial titanium (ASTM 265 B-2 Grade) was used in the investigation. The as-received material was in the form of a 5 mm thick sheet, and the chemical analysis and tensile properties are given in Table I. The as-received sheet was cold-rolled to 1 mm thickness following a schedule of about 1% reduction per pass on an average. During cold rolling, care was taken to see that the rolling direction (RD) was not altered from pass to pass. Sheet specimens with 4 mm gauge width and 15 mm gauge length were machined from the rolled sheet such that their tensile axes were either parallel to RD (longitudinal specimen) or perpendicular to RD (transverse specimen).

A few of the above specimens were edge-notched with the following notch dimensions: notch angle, 45°; notch depth, 1 mm; notch root radius, 0.1 mm.

A required number of machined specimens were annealed in a dynamic vacuum of 2.67×10^{-3} N m^{-2} at 1100 K for 2 h and subsequently furnace cooled. The resulting average grain diameter as measured by linear intercept method was 51 μm.

The following abbreviations describe the different types of specimens used in the investigation: A(L), annealed-longitudinal; A(T), annealed-transverse; CR(L), cold-rolled-longitudinal; CR(T), cold-rolled transverse.

2.2. Stress corrosion testing

The corrosion medium used was a solution containing 0.8 vol% bromine in methanol. These chemicals were of reagent grade. The water content of the medium, which was found [12] to play an important role in deciding the stress corrosion susceptibility, was analysed by the Karl Fischer method [13] and estimated to be less than 0.1 vol%.

The time to failure of the specimens immersed in the above medium and simultaneously stressed in tension was measured by loading the specimens in a constant load machine. This machine has features similar to Mayes Unisteel model MK 11 and has a lever ratio of 1 : 10. The time to failure was recorded using an electronic timer. The temperature of the medium was controlled to ± 0.5° with the help of a thermostat.

Some tensile experiments on specimens immersed in the medium, as well as in air, were also carried out on a constant cross-head speed tensile testing unit, at different cross-head speeds of 0.08, 0.4 and 2.0 mm min^{-1}.

2.3. X-ray diffraction and pole figures

The preferred orientations in the specimens were studied by X-ray techniques. The X-ray line intensities of different reflections were recorded on the rolling surface of the specimen mounted on a Philips diffractometer such that the RD was along or transverse to the X-ray beam. The integrated line intensities (I_{hkil}) for (0 0 0 2), (0 1 $\bar{1}$ 1), (0 1 $\bar{1}$ 2) and (1 0 $\bar{1}$ 3) reflections were calculated by taking them equal to the area under the intensity versus 2θ (θ = Bragg angle) curve. These were normalized with respect to the integrated line intensities (I_0) of the corresponding reflections recorded on a random specimen of annealed titanium powder. X-ray

TABLE I Chemical analysis and tensile properties of commercial titanium. L, longitudinal; T, transverse

Chemical analysis (wt%)						Tensile properties			
C	Fe	N	H	O	Ti		Yield strength (MPa)	Tensile strength (MPa)	Elongation (%)
						L	324	490	25
0.022	0.07	0.014	0.01	0.14	Bal	T	338	462	26

pole figures corresponding to (0 0 0 2) and (1 0 $\bar{1}$ 1) reflections were also recorded using the Schulz reflection technique [14] and a Philips texture goniometer. As the pole figures obtained by this technique will cover with accuracy only the central region (inclination angle of 0 to 70°), "composite" specimens with the thickness plane as the reflecting surface were prepared with a view to obtain the pole densities in the peripheral region. The "composite" specimens were prepared by slicing the sheet parallel to the longitudinal or transverse direction, into pieces with the width equal to their thickness and bonding them together closely such that the thickness plane becomes the reflecting surface. By combining the pole figure data obtained from the sheet specimen and the composite specimens, a complete pole figure covering inclination angles 0 to 90° was constructed.

3. Results

3.1. Time-to-failure data

The time taken by the specimens for failure (t_f) under SCC conditions is a function of applied tensile stress as shown in Fig. 1. The applied stress is expressed in terms of the percentage ultimate tensile strength (%UTS) of individual specimens. The annealed longitudinal, A(L), specimens take longer time for SCC failure than the corresponding A(T) at all stress levels. The specimens exhibited threshold stresses below which either SCC does not occur or take longer periods (40 h). The threshold stress for A(L) specimens is higher than that for the A(T) specimens. In Fig. 1, the arrows towards right indicate that the specimen did not fail up to about 40 h and is not likely to fail. The cold-rolled, both longitudinal and transverse, did not fail even at stresses as high as 80% of their UTS.

3.2. Apparent activation energy for SCC

The influence of temperature (T) in the range 295 to 325 K on t_f is shown in Fig. 2 in the form of an Arrhenius plot. The applied load was kept constant for a given type of specimen. However, it has been observed [12] that increasing stress levels will only shift the line parallel to itself without changing the slope. At a constant stress, $\log(t_f)$ varies linearly with $(1/T)$ and follows an equation of the type:

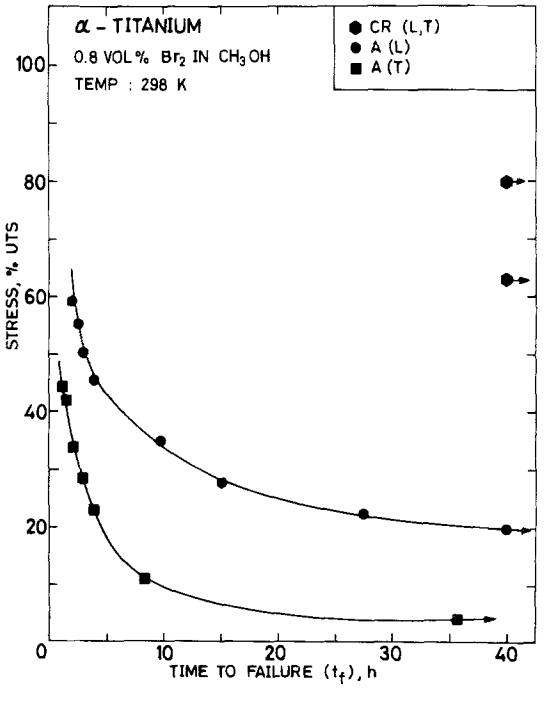

Figure 1 Variation of time to failure with % UTS at 298 K in annealed titanium (longitudinal and transverse). The data points for cold-rolled specimens that did not fail are also shown. The arrows toward right indicate that these specimens did not fail and will take longer periods.

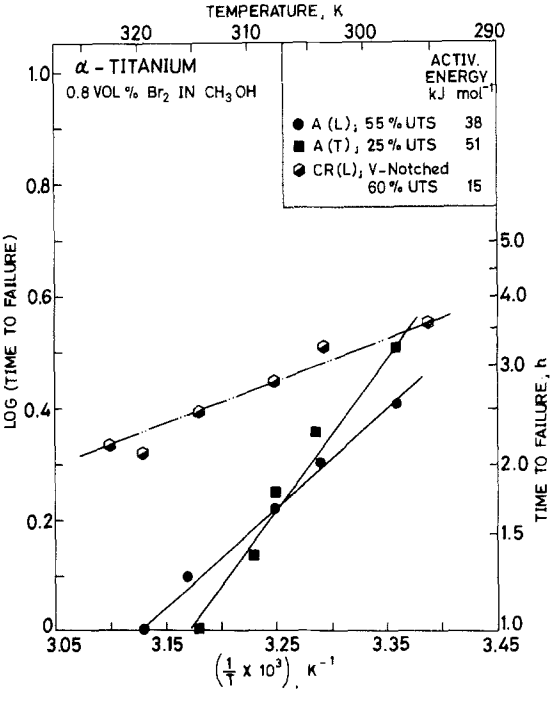

Figure 2 Arrhenius plot between the time-to-failure and temperature for annealed titanium (longitudinal and transverse). The data for notched specimens of cold-rolled longitudinal specimens are also shown.

TABLE II Apparent activation energy for different types of specimens used in the investigation

Specimen	Stress level (% UTS)	Apparent activation energy ($\pm$ 5 kJ mol^{-1})
A(L)	55	38
A(T)	25	51
CR(L)-notched	60	15

$$(1/t_f) = A \exp(-Q/RT), \qquad (1)$$

where A = constant, Q = activation energy for SCC, T = absolute temperature, and R = gas constant. The activation energy (apparent) estimated from the slope of $\log(t_f)$ versus $(1/T)$ plot for different types of specimens is given in Table II. The stress levels chosen for the evaluation of apparent activation energy were such that the time to failure is within about 4 h.

The cold-rolled specimens did not fail at any temperature in the range studied. However, these specimens failed when notched, in times comparable with those of the annealed specimens. The apparent activation energy estimated on the notched cold-rolled longitudinal specimens is listed in Table II.

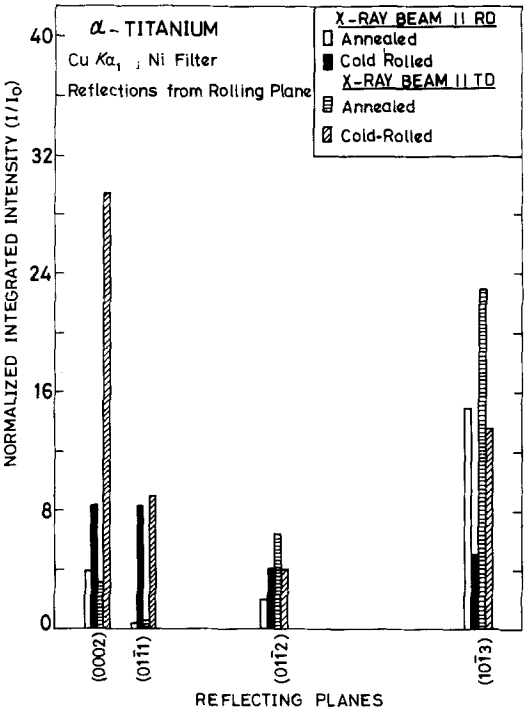

Figure 3 Normalized X-ray line intensity (I_{hkil}/I_0) data for annealed and cold-rolled titanium. The values obtained when RD is along the X-ray beam as well as when TD is along the X-ray beam are included.

3.3. Tensile test data at constant cross-head speeds

The results obtained on the dynamic tests at constant cross-head speeds are given in Table III. In the table are given the data obtained on specimens deformed in air and in medium. A comparison of the data on A(L) shows the elongation is drastically reduced at the cross-head speed of 0.08 mm min^{-1} while the specimen is immersed in the medium. A similar behaviour is also shown by the annealed transverse specimen except that the reduction in elongation at lower cross-head speeds is more marked in the presence of corrosive medium. The CR(L) specimens did not suffer any loss in elongation in the medium with decreasing cross-head speed. However, a slight increase in the yield stress and UTS have been observed, particularly at lower cross-head speeds, when the tests were performed in the medium.

3.4. Texture

The values of the normalized integrated X-ray line intensities (I_{hkil}/I_0) for (0 0 0 2), (0 1 $\bar{1}$ 1), (0 1 $\bar{1}$ 2) and (0 1 $\bar{1}$ 3) reflections are given in

TABLE III Tensile data on α-titanium obtained by testing in air and bromine–methanol solution

Specimen	Cross-head speed (mm min^{-1})	0.2% yield stress (MPa)		UTS (MPa)		Elongation (%)	
		Air	Medium	Air	Medium	Air	Medium
A(L)	2.0	333	300	486	395	23	20
	0.4	321	243	495	357	24	16
	0.08	276	251	479	286	23	5
A(T)	2.0	334	328	461	402	23	22
	0.4	328	297	458	390	21	17
	0.08	310	262	437	345	20	4
CR(L)	2.0	688	681	804	816	1.8	1.7
	0.4	666	695	806	831	1.7	1.8
	0.08	640	694	814	891	1.8	1.6

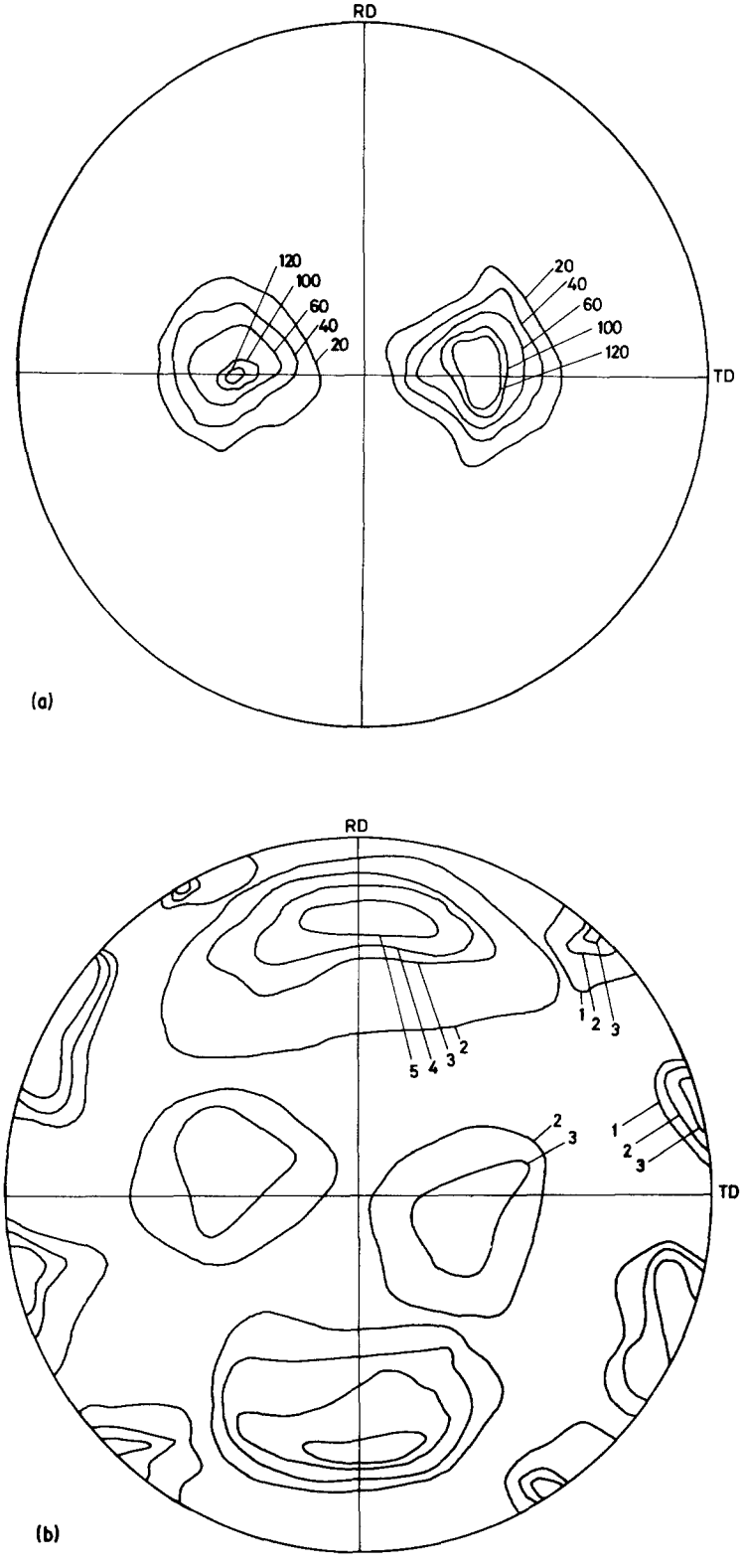

Figure 4 (a) $\{0\ 0\ 0\ 2\}$ pole figure for annealed titanium. RD, rolling direction, TD, transverse direction. (b) $\{1\ 0\ \bar{1}\ 1\}$ pole figure for annealed titanium. RD, rolling direction, TD, transverse direction.

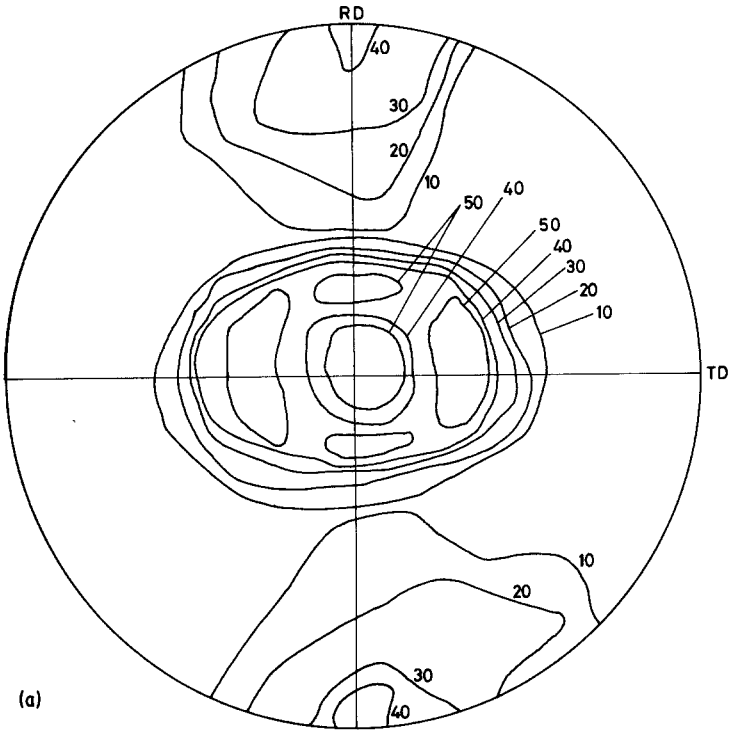

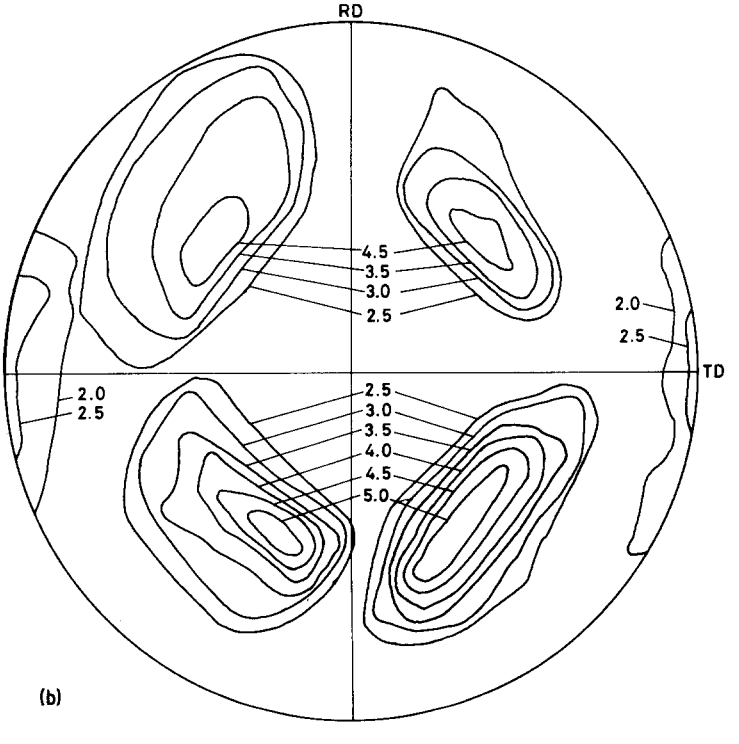

Figure 5 (a) $\{0\ 0\ 0\ 2\}$ pole figure for cold-rolled titanium. (b) $\{1\ 0\ \bar{1}\ 1\}$ pole figure for cold-rolled titanium.

Fig. 3. These were obtained on annealed as well as cold-rolled titanium. Two sets of data are represented in Fig. 3: one obtained when the X-ray beam is along RD and the other when the X-ray beam is along transverse direction (TD). As the sample has preferred orientation or texture, these two sets have different (I_{hkil}/I_0) values. The cold rolling has increased the (0 0 0 2), (0 1 $\bar{1}$ 1) and (0 1 $\bar{1}$ 2) intensities when the X-ray beam is along RD, while the (0 1 $\bar{1}$ 3) intensity has decreased. Similar changes occurred when the X-ray beam was along TD, except in the case of (0 1 $\bar{1}$ 2) the value for which is slightly lowered on cold rolling.

The {0 0 0 2} and {1 0 $\bar{1}$ 1} pole figures recorded on annealed and cold-rolled materials are given in Figs. 4 and 5, respectively. The iso-intensity contours are marked as multiples of random units. Referring to Fig. 4a, the annealed titanium is strongly textured and an intense {0 0 0 2} peak appears at about 30 to 35° from the sheet normal (SN) towards TD. This matches well with the earlier results [8]. The {1 0 $\bar{1}$ 1} pole figure for annealed titanium (Fig. 4b) shows that the peak intensity occurs at about 20 to 25° from RD towards SN.

The {0 0 0 2} pole figures for the cold-rolled titanium (Fig. 5a) shows strong peaks at SN, 25 to 30° from SN towards TD as well as RD, and at RD. In general, the {0 0 0 2} poles are concentrated around SN in addition to the peak at RD. The {1 0 $\bar{1}$ 1} peaks (Fig. 5b) are symmetrically situated in the four quadrants of the pole figure.

Comparing the {0 0 0 2} pole figure on annealed titanium (Fig. 5a), it is clearly seen that the texture is considerably changed by cold rolling – a peak around SN and one at RD are produced. The {1 0 $\bar{1}$ 1} pole figures (Figs. 4b and 5b) for these two materials show a difference.

3.5. Fractography

The scanning electron micrographs recorded on the fracture surface of A(L) and A(T) specimens failed in constant load tests are shown in Fig. 6. The crack initiation occurs on the thickness plane and the propagation is along an intercrystalline path in the initial stages. When the effective cross-section is reduced by the propagating crack, the final separation occurs by mechanical fracture (indicated by dimple formation). The CR(L) and CR(T), both in notched condition, showed cleavage even at a distance of 1 mm from the notch (Fig. 7). The fracture surface is viewed such that the electron beam is normal to it and the location of the micrographs is indicated schematically in Fig. 7.

4. Discussion

4.1. Mechanism of SCC in annealed titanium

The time to failure, t_f, in a constant load SCC test consists of several components: (i) time taken for crack initiation, t_i, (ii) time taken for crack propagation, t_p, and (iii) time taken for final mechanical separation, t_m, such that:

$$t_f = t_i + t_p + t_m. \quad (2)$$

The value of t_m is decided by the process of stress rupture and is considered [15] to be much smaller in comparison with t_f. Also, the value of t_m is likely to be the same for both A(L) and A(T), since the tensile properties in these two directions are not largely different (Table III). The time taken for crack propagation depends on the chemistry of the solution, the electrochemical behaviour, the applied stress, the microstructure and the mode of failure. In annealed titanium tested in longitudinal and transverse directions, the value of t_p will be clearly identical for similar experimental conditions since the microstructure (equi-axed grain structure) and mode of failure (intergranular) are essentially the same (Fig. 6). Thus the difference in time to failure for L and T samples can be attributed only to the differences in crack-initiation period. It is observed that the dominant crack causing SCC failure is initiated on the thickness plane and hence the passivation characteristics of this plane assume considerable importance. The protective nature of the passivating film under stress is related to the chemical reactivity of the thickness surface which depends on the crystallography of this plane. From the texture identified for annealed titanium (Fig. 4) the thickness plane in the case of longitudinal specimen will be {1 0 $\bar{1}$ 1} while that for the transverse specimen will be {1 1 $\bar{2}$ 0}, as can be visualized from a schematic block diagram shown in Fig. 8a. The chemical reactivity of the planes is dependent on the atomic configurations of these planes and the single-crystal data recorded on different planes showed [16] that the corrosion rate increases in the sequence {0 0 0 1}< {1 1 $\bar{2}$ 2}< {1 1 $\bar{2}$ 0}. The chemical reactivity is thus related to the atomic density of the plane. The spherical ball models of atomic arrangements for {1 0 $\bar{1}$ 1} and {1 1 $\bar{2}$ 0} planes are given by

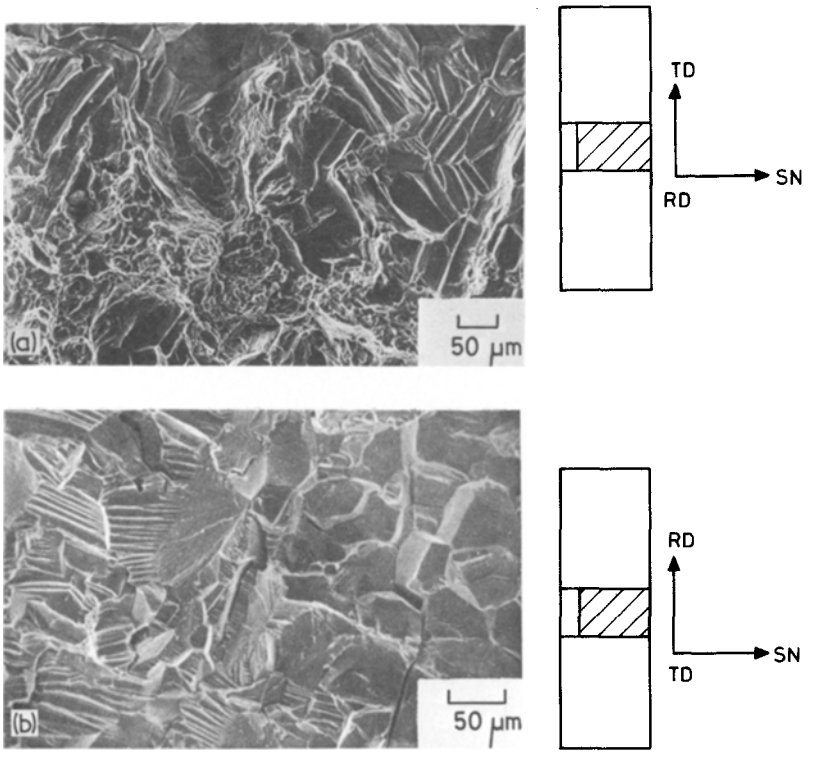

Figure 6 Scanning electron micrographs of specimens failed in constant load SCC test on annealed titanium. (a) Longitudinal, (b) transverse. The location of the photographs on the fractured surface is schematically indicated.

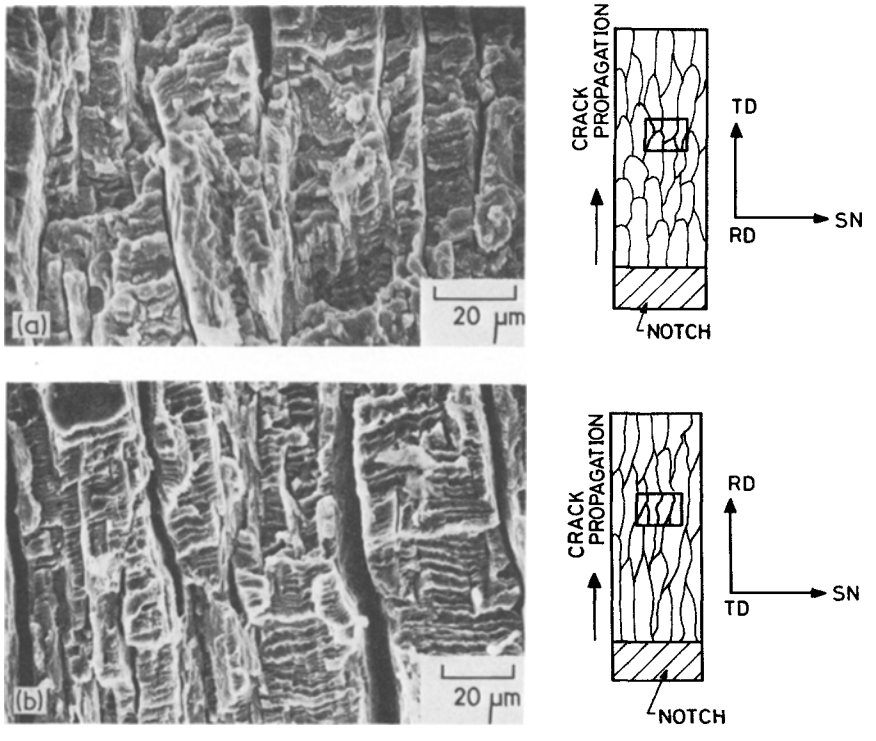

Figure 7 Scanning electron micrographs of notched specimens of (a) cold-rolled-longitudinal, and (b) cold-rolled-transverse titanium specimens failed in SCC. The location of the photographs on the fractured surface and the grain structure are schematically indicated.

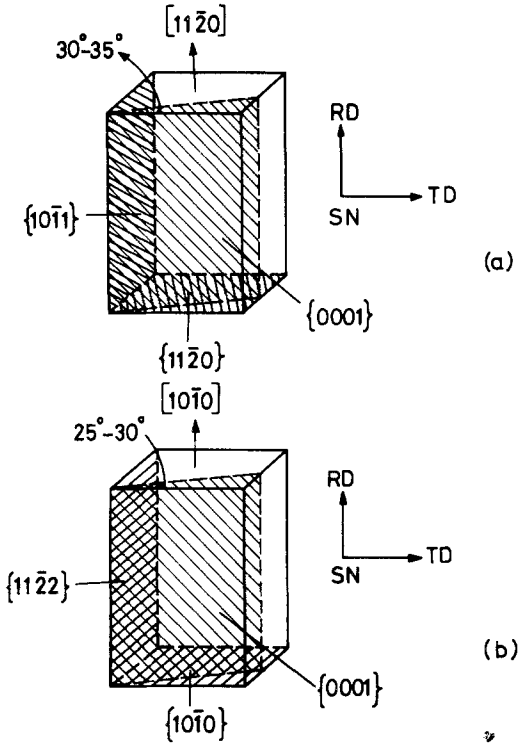

Figure 8 Schematic diagram to show the indices of the thickness plane corresponding to the identified textures in titanium (a) annealed, (b) cold-rolled.

Rosenbaum [17]. The $\{1\,1\,\bar{2}\,0\}$ surface is a deeply grooved surface composed of zig-zag chains of atoms which are not in contact with each other, while the $\{1\,0\,\bar{1}\,1\}$ is comparatively better close packed with the different atoms touching each other. As the passivation and repassivation characteristics are better on a densely packed plane, the longitudinal specimen will take longer time for stress corrosion crack initiation compared with the transverse specimen.

The difference in apparent activation energy values obtained for L and T specimens (Table II) can be attributed to the change in t_i values for these two types of specimens. As the apparent activation energy is estimated from the variation of the *total* time to failure with temperature, an increase in the crack initiation period, Δt_i, as in the case of longitudinal specimen, can cause a decrease in the slope of $\log(t_f)$ versus $(1/T)$ and thereby decrease the apparent activation energy. Moreover, there are two limitations in determining the apparent activation energy values: (1) the temperature range of study is limited by the low boiling point of the corrodant, (2) the mode of failure may not be of one type completely throughout the distance of crack propagation and some mixed modes may occur when the crack grows longer. It is difficult to have only one mode of failure in a constant load test.

The range of apparent activation energy (33 to 51 kJ mol^{-1}) observed in annealed materials suggests a mechanism of stress-aided anodic dissolution at the grain boundaries since the activation energy for this mechanism ($\approx$ 50 kJ mol^{-1}) [18] falls within this range. The activation energy reported by Haney *et al.* [19] (39 kJ/mol^{-1}) and Hoar and West [20] (25 kJ mol^{-1}) are also very near this value. The mechanism of stress-aided anodic dissolution is further supported by the electrochemical measurements [12].

4.2. Mechanism of SCC in cold-rolled titanium

The cold-rolled titanium sheet has developed considerable resistance to SCC in bromine–methanol solution. The effect of cold work on the SCC characteristics will be through the following factors: (i) stored energy of cold work and dislocation structures, and (ii) preferred orientations – both crystallographic texture and grain-boundary orientations. If the stored energy of cold work and increased dislocation density are responsible for the increased resistance to SCC, the resistance should be developed in the specimen irrespective of the type of cold work to which it is subjected. This is not found to be true [11] since the specimens deformed by giving only tensile strains have not developed any resistance to SCC. Furthermore, it was reported [21] in steel that cold working actually increases the susceptibility to SCC in NaCl solutions. In view of these conditions, it is necessary to examine the effect of preferred orientations on the SCC behaviour of α-titanium. The microstructural anisotropy (elongation of grains in RD) cannot be held responsible for the resistance developed as this should give SCC susceptibility when tested in the transverse direction. The role of texture in the SCC behaviour of cold-rolled titanium is, therefore, to be considered.

The pole figures for the cold-rolled titanium (Fig. 5) when compared with those for annealed titanium (Fig. 4) clearly show that the texture in these two cases are widely different. The resistance to SCC developed by cold rolling may be related to the crystallographic texture in terms of the passivation characteristics of the thickness plane.

Considering that the $\{0\,0\,0\,2\}$ peak at 30° away from SN towards TD and RD to be $[1\,0\,\bar{1}\,0]$, the thickness plane for CR(L) specimen will be $\{1\,1\,\bar{2}\,2\}$ while that for CR(T) will be $\{1\,0\,\bar{1}\,0\}$. The $\{1\,0\,\bar{1}\,0\}$ plane is one of the slip planes while $\{1\,1\,\bar{2}\,2\}$ is a twinning plane in titanium. Both these planes are densely packed and can cause effective passivation and repassivation under stress.

The resistance to SCC in the cold-rolled specimens is due to a difficulty either in the nucleation of stress corrosion cracks or in their subsequent propagation towards a final failure. The observation that notched specimens have failed suggests that the delay in crack initiation is responsible for the SCC resistance. This delay in crack initiation is due to the texture as explained above. The presence of notch in cold-rolled material gives stress concentration at the notch tip and increases the tensile stress component so as to facilitate the crack propagation. In addition, from Fig. 7b it can be visualized that both prismatic and basal slip planes are unfavourable for slip in both the cases and hence repassivation is faster than the film rupture by plastic deformation. This prevents the crack initiation.

The mode of failure in the case of cold-rolled notched specimens was cleavage (Fig. 7). The apparent activation energy ($15\,kJ\,mol^{-1}$) indicates a mechanism based on hydrogen embrittlement since this value is close to that required for diffusion of hydrogen in α-titanium and its alloys [18] ($18.5\,kJ\,mol^{-1}$). Atomic hydrogen is generated due to cathodic reactions at the crack tip and diffuses into the matrix. As this diffusion is enhanced by cold work [22], the hydrogen embrittlement assumes importance in cold-rolled titanium. The presence of hydrogen at the crack tip can cause embrittlement in the following two ways: (i) diffusion of atomic hydrogen causing embrittlement, and (ii) forming hydrides on certain crystallographic planes (habit planes) and causing cleavage. As the favoured cleavage planes are normal to the tensile axis, from the known cold-rolling textures it is possible to arrive at the probable cleavage planes. In the case of CR(L) specimen, the planes normal to the tensile axis are $\{0\,0\,0\,2\}$ or close to that (possibly $\{1\,0\,\bar{1}\,7\}$ or $\{1\,0\,\bar{1}\,8\}$) if the $\{0\,0\,0\,2\}$ peak at RD is taken into consideration (Fig. 5a). If the $\{0\,0\,0\,2\}$ peak at 30° from SN towards TD is considered, the cleavage planes will be near $\{1\,0\,\bar{1}\,0\}$. For the CR(T) specimen, on the other hand, the cleavage planes will be close to $\{1\,1\,\bar{2}\,2\}$. All these cleavage planes are known to be possible habit planes for hydride formation in α-alloys [23–26]. The scanning micrographs given in Fig. 7 show, in addition to cleavage, stable discontinuous cracks almost parallel to the direction of propagation of transcrystalline crack. As no grain-boundary attack was noticed on the surface of the specimen, these cracks might have formed during the transcrystalline crack propagation itself when the solution seeps in and attacks freshly exposed grain boundaries. Since the sheet is cold-rolled, the grains are elongated in the rolling direction and the resulting grain structures at the fracture surface in the longitudinal and transverse specimens are shown schematically in Fig. 7. The cracks seen in the micrographs appear to be the grain-boundary cracks and are stable but discontinuous. These, however, have not taken part in the process of SCC failure by cleavage because of their unfavourable orientation. The steps that are seen in the micrographs are caused during the advancement of the crack leading to failure and are distinctly different from the flutings that occur in the SCC failures of annealed zirconium and titanium materials [27]. It may be noted that flutings will not readily occur in textured materials since cleavage planes will be closely aligned to facilitate crack propagation.

The data obtained from the tensile tests at constant cross-head speed are also in support of the above explanations for the behaviour of annealed and cold-rolled titanium. The slight increase in the yield strength and UTS at lower cross-head speeds ($0.08\,mm\,min^{-1}$) in the cold-rolled titanium (Table II) would have resulted from the formation of a strong, adherent and quickly repairable passivating film while the loss in ductility in the annealed titanium is a consequence of the intergranular crack propagation being faster than the repassivation.

5. Conclusions

(1) The SCC characteristics of α-titanium in 0.8 vol% bromine in methanol are different in L and T directions, the A(L) specimen having better resistance. The difference is attributed to the change in the passivation characteristics of the edge plane brought about by a change in their crystallography.

(2) The apparent activation energy estimated in annealed specimens lies between 30 and

51 kJ mol^{-1} which, considered along with the electrochemical behaviour, suggests a mechanism of stress-aided anodic dissolution. The apparent activation energy was found to be texture dependent.

(3) The cold-rolled titanium developed resistance to SCC and when tested with a notch showed a cleavage failure. This resistance was related to the texture in terms of the ready passivation of the crystallographic planes parallel to the thickness plane.

(4) The apparent activation energy for cold-rolled longitudinal notched specimens (15 kJ mol^{-1}) suggests a mechanism of hydrogen embrittlement. The cleavage planes deduced from the texture data matched with the suggested habit planes for titanium hydride.

Acknowledgements

The authors gratefully acknowledge the authorities of National Aeronautical Laboratory, Bangalore, Indian Institute of Technology, Madras and Central Electrochemical Research Institute, Karaikudi for kindly extending their SEM, X-ray goniometer and potentiostatic facilities, respectively. In particular, the authors place on record their appreciation for the help rendered by Dr R. V. Krishnan (NAL), Mr Keshavan Nair (IIT) and Mr N. S. Rengaswamy (CECRI) during this investigation.

References

1. M. J. BLACKBURN, J. A. FEENY and T. R. BECK, "Advances in Corrosion Science and Technology", Vol. 3 (Plenum Press, New York, 1973) p. 67.
2. A. J. SEDRIKS, J. A. S. GREEN and P. W. SLATTERY, *Corrosion* **24** (1968) 172.
3. A. J. SEDRIKS and J. A. S. GREEN *ibid* **25** (1969) 324.
4. T. R. BECK, in "The Theory of Stress Corrosion Cracking in Alloys" edited by J. C. Scully (Maney, UK, 1971) p. 64.
5. J. SPURRIER and J. C. SCULLY, *Corrosion* **28** (1972) 453.
6. J. BRETTLE, *Metals and Materials* **6** (1972) 442.
7. R. J. H. WANHILL, *Acta Met.* **21** (1973) 1253.
8. F. LARSON and A. ZARKADES, "Properties of Textured Titanium Alloys", MCIC-74-20, Battelle Columbus Laboratory, Columbus, Ohio (1974).
9. D. N. FAGER and W. F. SPURR, *Trans. ASM Q.* **61** (1968) 283.
10. R. R. BOYER and W. F. SPURR, *Met. Trans.* **9A** (1978) 1443.
11. H. V. SUDHAKER NAYAK, K. I. VASU and Y. V. R. K. PRASAD, *Scripta Met.* **12** (1978) 869.
12. *Idem, J. Electrochem. Soc. India* **27** (1978) 95.
13. A. I. VOGEL, "A Text Book of Quantitative Inorganic Analysis", 3rd Edn. (E.L.B.S., London, 1964) p. 944.
14. L. G. SCHULZ, *J. Appl. Phys.* **20** (1949) 1030.
15. C. J. McMAHON, Jr and D. J. TRAUX, *Corrosion* **29** (1973) 47.
16. J. A. S. GREEN, *ibid.* **30** (1974) 175.
17. H. S. ROSENBAUM, "Deformation Twinning" (Gordon and Breach, New York, 1964) p. 43.
18. M. J. BLACKBURN and W. H. SMYRL, "Titanium Science and Technology", Vol. 4 (Plenum Press, New York, 1973) p. 2577.
19. E. G. HANEY, R. GOLDBERG, R. ERNSBERGER and W. T. BREHM, Rept. No. 2 (NGR-39-008-014), Mellon Institute (1967).
20. T. P. HOAR and J. WEST, *Proc. Roy. Soc.* **A268** (1962) 304.
21. T. P. HOAR, in "The Theory of Stress Corrosion Cracking in Alloys" edited by J. C. Scully (Maney, UK, 1971) p. 105.
22. D. T. POWELL and J. C. SCULLY, *Corrosion* **25** (1969) 483.
23. I. W. HALL, *Met. Trans.* **9A** (1978) 815.
24. G. SANDERSON and J. C. SCULLY, *Trans. AIME* **239** (1967) 1883.
25. J. D. BOYD, *Trans. ASM* **62** (1969) 971.
26. T. S. LIU and M. A. STEINBERG, *ibid* **50** (1958) 455.
27. I. AITCHISON and B. COX, *Corrosion* **28** (1972) 83.

Received 28 September and accepted 23 October 1979.